

Fabrication of Solid-State Dye-Sensitized Solar Cells by Controlled Evaporation of Solvents for Creation of Facile Charge Transport Pathway

Yuki Kurokawa, Takehito Kato, and Shyam S. Pandey*

Solid-state dye-sensitized solar cells (ss-DSSCs) based on MK-2 dye-sensitized TiO_2 photoanode and the most commonly used I^-/I_3^- redox electrolyte are successfully fabricated by the simple method of solidification of the injected liquid electrolyte under slow solvent evaporation. The use of the ionic liquid, which is solid at room temperature, and slow evaporation of solvent at low temperature is a key step for solidification toward the fabrication of ss-DSSCs. It has been demonstrated that ss-DSSCs thus fabricated not only retain about 80% of photoconversion efficiency (PCE) as compared to their liquid-state DSSCs counterpart but also maintain the device stability for more than 1000 h. PCE of the ss-DSSCs is found to increase as a function of the increasing concentration of the ionic liquid used for electrolyte preparation. In the case of ss-DSSCs with the ionic liquid concentration of 1.2 M, there is a good balance between PCE and durability leading to not only retention of about 70% of PCE as compared to its liquid-state DSSCs counterparts but also maintaining the stability of the solar cell for more than 1000 h stored at room temperature.

1. Introduction

Among renewable energy resources, solar energy available as a free gift to us from nature has the capability to provide the singular solution for all of our future energy demands.^[1] The installation of solar cells for energy harvesting is the most attractive method because it easily converts solar energy into directly usable electrical energy. Although the installation of silicon-based solar panels continues to increase around the world, its high cost of electricity


production is one of the bottlenecks to competing with the other power generation methods based on fossil fuels, which is needed for its reach to the common mass level. Therefore, there is a worldwide effort to direct their focus on the development of next-generation solar cells, which are also known as third-generation solar cells such as dye-sensitized solar cells (DSSCs), organic thin-film polymer solar cells, and recently came to the limelight organic-inorganic hybrid perovskite solar cells, as low-cost alternatives to the commercial silicon-based solar cells currently in use.^[2–4] These solar cells are lightweight and flexible, use less-inexpensive raw materials, do not require high temperatures and vacuum to create ultrapure materials, and do not require high energy-consuming processes making energy payback time relatively small.^[5] Among next-generation solar

cells, DSSCs are attracting great attention for use in a wide range of fields such as indoor light usage for Internet of Things (IoT) power sources, low manufacturing cost, esthetic beauty, vivid colors, transparency to make their suitability as colorful power harvesting windows and last but not least due their extremely good performance under low light conditions.^[6]

DSSCs consist of a working electrode containing sensitizing dye adsorbed on porous nanocrystalline and mesoporous titanium dioxide (TiO_2) coated on transparent conductive oxide (TCO) substrate, a conductive counter electrode with a catalytic layer, and a redox electrolyte that fills the space between them. In order to challenge existing commercial silicon-based solar cells, it is essential to solve key issues such as further improving photoconversion efficiency (PCE), reducing manufacturing costs and improving long-term environmental stability. Various recent efforts in the scientific community have been directed to the use of ruthenium-free organic dyes, the removal of expensive transparent conductive oxides, and low-cost Pt-free catalyst for the counter electrodes.^[7–13] The development of dyes having a wide photon harvesting range suitable for power generation designed from the perspective of molecular engineering and the use of electrolytes consisting of redox pairs with deeper redox potentials led to the achieving over 12% efficiency of DSSCs, which exceeds the efficiency of amorphous silicon.^[14–17] Among the various components of a DSSC, the electrolyte provides an important role in completing the DSSC's working cycle by transporting electrons reaching the counter electrode via the

Y. Kurokawa, S. S. Pandey
 Graduate School of Life Science and Systems Engineering
 Kyushu Institute of Technology
 2-4, Hibikino, Wakamatsu, Kitakyushu, Fukuoka 808-0196, Japan
 E-mail: shyam@life.kyutech.ac.jp

T. Kato
 National Institute of Technology
 Oyama College
 Oyama, Tochigi 323-0806, Japan

 The ORCID identification number(s) for the author(s) of this article can be found under <https://doi.org/10.1002/pssa.202300116>.

© 2023 The Authors. physica status solidi (a) applications and materials science published by Wiley-VCH GmbH. This is an open access article under the terms of the Creative Commons Attribution-NonCommercial-NoDerivs License, which permits use and distribution in any medium, provided the original work is properly cited, the use is non-commercial and no modifications or adaptations are made.

DOI: 10.1002/pssa.202300116

redox reaction to the oxidized dye molecule, which regenerates the dye molecule. However, in the high-performance DSSCs reported so far, the most commonly used electrolyte is the liquid electrolytes consisting of redox pair based on iodine and cobalt complexes dissolved in a volatile organic solvent like acetonitrile. However, there are concerns about the negative effects on the environment and human health in the case of liquid electrolyte leakage, especially iodine-based redox electrolytes. Another concern is its durability because the evaporation of solvent from liquid electrolytes makes the DSSCs no longer function and a lot of research focuses have been directed to circumvent this issue.^[18]

Existing solid-state (ss)-DSSCs in which the electrolyte is replaced by a hole-transporting material also require them to infiltrate the mesoporous TiO_2 layer homogeneously.^[19] However, it is very difficult to use polymer materials such as poly(3-hexylthiophene-2,5-diyl) (P3HT) are extremely difficult to use owing to their bulky size. The efforts have been directed toward the photoelectrochemical polymerization of monomers that can easily penetrate nanopores to provide a solution for filling polymers with fairly large sizes, which are particularly difficult for electrolyte penetration. However, utilization of such methods is cumbersome and seems not industrially viable, especially for the production of large-area modules.^[20] Although there have been reports using Spiro-MeOTAD, a relatively low molecular weight hole transport material, its PCE is always lower than liquid state DSSCs, and its use of metal electrodes means that the advantage of the bifacial structure of DSSCs disappears.^[21,22] In ss-DSSC, cobalt-based electrolytes, copper complex electrolytes, and other electrolytes, which are expected to have larger open-circuit voltages than typical iodine-based electrolytes, have also been researched and reported high PCEs.^[23,24] However, the recombination due to reverse electron transfer is intense because these redox pairs consist of cations, which attract electrons diffusing into TiO_2 . Therefore, these electrolytes can only be applied to a limited number of dyes. In this present work, efforts were directed to fabricate the ss-DSSCs by first fabricating conventional liquid-state DSSCs followed by slow solidification by natural evaporation

of the solvent of the iodine-base liquid electrolyte leading to solidification. It has been demonstrated that by this simple method, not only 60–70% of the PCE was retained in the ss-DSSCs but it also imparted durability to the ss-DSSCs for more than 1000 h. The effect of ionic liquid concentration on the performance of the ss-DSSCs this fabricated was also examined systematically.

2. Experimental Section

2.1. Materials

4-*tert*-butylpyridine (*t*BP) was purchased from Sigma–Aldrich. Lithium iodide (LiI) and iodine (I_2) were purchased from Wako, Japan. MK-2 dye was purchased from Soken Chemical & Engineering. TiO_2 paste (Ti-nanoxide R/SP) and platinum catalyst precursor (Platisol T) were purchased from Solaronix. TiO_2 paste (30NRD) was purchased from Catalysts and Chemicals (Japan). 1,2-dimethyl-3-propylimidazolium iodide (DMPH) was purchased from TCI Chemicals, Japan.

2.2. Preparation of Working Electrodes

Fluorine-doped tin oxide (FTO) glass substrate ($15 \Omega \text{ sq}^{-1}$) was cleaned ultrasonically followed by the UV/O_3 treatment for 30 min. The substrates were dipped in a 40 mM TiCl_4 aqueous solution at 70°C for 1 h, and then rinsed with distilled water and ethanol. After rinsing, treated substrates were sintered at 500°C for 45 min in a muffle furnace (FO100, Yamato Co., Ltd.). Screen-printable transparent TiO_2 paste (30NRD) and opaque TiO_2 paste (Ti-nanoxide R/SP) were screen-printed on TiCl_4 -treated substrate and sintered at 500°C for 45 min in a muffle furnace resulting in $8 \mu\text{m}$ -thick TiO_2 layer. The TiO_2 -coated glass substrates were again treated with TiCl_4 followed by sintering as discussed above. After TiCl_4 treatment, the substrates were dipped in 0.3 mM of MK-2 dye in toluene solution overnight followed by rinsing with the same solvent to remove the unadsorbed dye

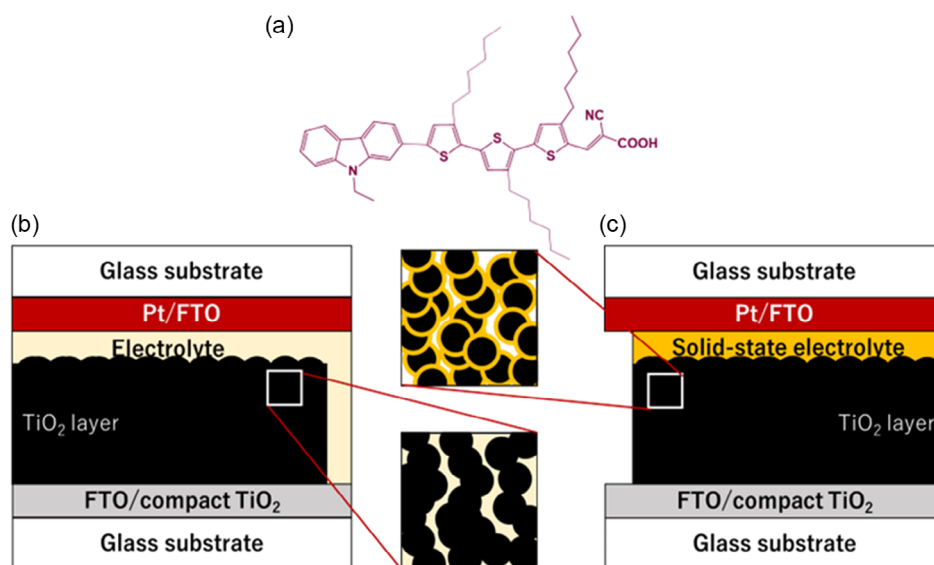


Figure 1. a) Molecular structure of sensitizing dye MK-2 and schematic cross-sectional view of b) liquid-state DSSC and c) solid-state DSSC.

molecules. The chemical structure of the MK-2 dye used in this work is shown in Figure 1.

2.3. Preparation of Counter Electrodes

Predrilled FTO glass substrates were cleaned under sonication by using ethanol, acetone, and 2-propanol for 10 min each followed by UV/O₃ treatment for 10 min. Platinum catalyst precursor (Platisol T) was spin-coated at 1400 rpm for 10 s on the FTO glass substrates and was sintered at 500 °C for 30 min in a muffle furnace.

2.4. Fabrication of Liquid/Solid-State DSSCs

The prepared working electrode and counter electrode were directly fixed together by UV curable resin (Three-Bond, Japan). An iodine-based redox electrolyte was injected through a predrilled hole on the counter electrode. The composition of the electrolyte was 0.05 M I₂, 0.1 M LiI, 0.5 M *t*BP, and 0 to 3.0 M DMPII dissolved in acetonitrile. After injection, the two holes were sealed with UV-curing resin to make liquid-state DSSCs. After the photovoltaic measurement of DSSCs based on liquid electrolyte, the sealing was removed and stored in a cool dark place for 72 h to form a solid electrolyte by natural drying of acetonitrile solvent. Schematic representations for the solid- and liquid-state DSSCs are shown in Figure 1.

2.5. Device Characterization

For the solar cell performance evaluation, photocurrent density–voltage (*J*–*V*) curves were measured using AM1.5G solar simulator (PEC-L01, Peccell, Japan) for the standard incident light source and a source-measure unit (Keithley 6400). The intensity of light was calibrated to 100 mW cm^{−2} with a standard silicon photodiode. Incident photon to current efficiency (IPCE) spectrum was measured with an exposure of constant photon flux of 1 × 10⁶ photon cm^{−2} in DC mode by using CEP-2000 (Bunko Keiki, Japan).

3. Results and Discussion

3.1. Photovoltaic Performance of Liquid-State and Solid-State DSSCs

Photovoltaic performance of DSSCs fabricated using the most commonly used iodine-based redox electrolyte in the liquid state (just after fabrication and electrolyte injection) and ss-DSSCs fabricated by natural evaporation of acetonitrile solvent after 72 h for solidification were measured after simulated 1 Sun light irradiation. The *J*–*V* curves for both the liquid-state and ss-DSSCs are shown in Figure 2. After simulated solar irradiation, liquid-state DSSCs exhibited photovoltaic parameters such as short-circuit current density (*J*_{sc}), open-circuit voltage (*V*_{oc}), and fill factor (FF) of 12.6 mA cm^{−2}, 0.70 V and 0.61 leading to a PCE of 5.41%. On the other hand, in the case of ss-DSSCs, photovoltaic performance was reduced with photovoltaic parameters such as *J*_{sc}, *V*_{oc}, FF, and PCE estimated to be 8.16 mA cm^{−2}, 0.66 V, 0.61, and 3.26%, respectively, and there was the retention of the 60% of photovoltaic performance as compared to that of liquid-state

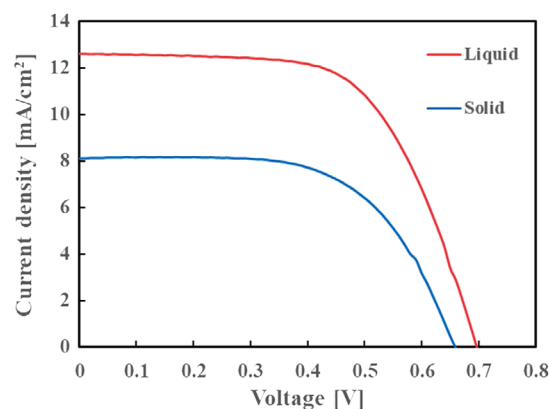


Figure 2. Photovoltaic performance of liquid-state DSSC and ss-DSSCs obtained after 72 h of slow solvent evaporation at room temperature for electrolyte solidification. The concentration of the ionic liquid DMPII used was 0.6 M.

DSSC after the 72 h of the natural solvent evaporation when the acetonitrile solvent is expected sufficiently evaporated and it was considered to be ss-DSSCs.

Although FF for both the liquid-state and ss-DSSCs was almost the same (0.61), however, it was also observed that the values of *V*_{oc} and *J*_{sc} decreased for the ss-DSSCs. This decrease in *V*_{oc} is considered to be due to the evaporation of *t*BP contained in the electrolyte. On the other hand, the large decrease of *J*_{sc} is considered to be caused by the discontinuity of the electrolyte layer owing to solidification. In the liquid state, electron transfer is carried out by ion exchange between I[−] and I₃[−] ions in liquid electrolyte via redox reaction allowing facile ion transport and dye-regeneration. However, the ions no longer diffuse in the solid state, and the transfer of electrons is considered to be carried out by the Grotthuss mechanism^[25,26] in which I[−] and I₃[−] ions adjacent to each other inside a continuous polyiodide layer transport electron working as a whole transport layer transferring the generated holes after dye-regeneration by hopping, which has been schematically shown in Figure 3.

One of the main reasons for the need for solidification is to enhance the durability of DSSCs as described in the introductory section. This consideration indicates that the solvent evaporation after 72 h works as well as ss-DSSC and the elapsed time beyond that indicates the stability of the ss-DSSC produced in this study. The changes in PCE with the storage time of the

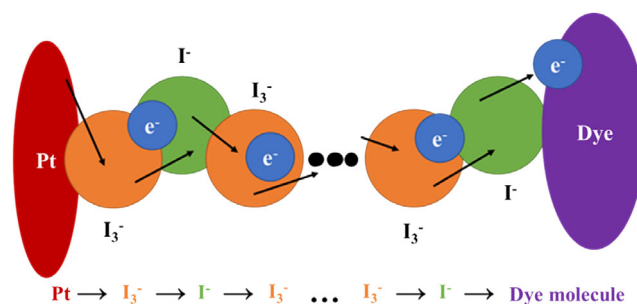


Figure 3. Schematic representation of electron transport and hole transfer from dye molecule to Pt counter electrode via solid-electrolyte in ss-DSSC.

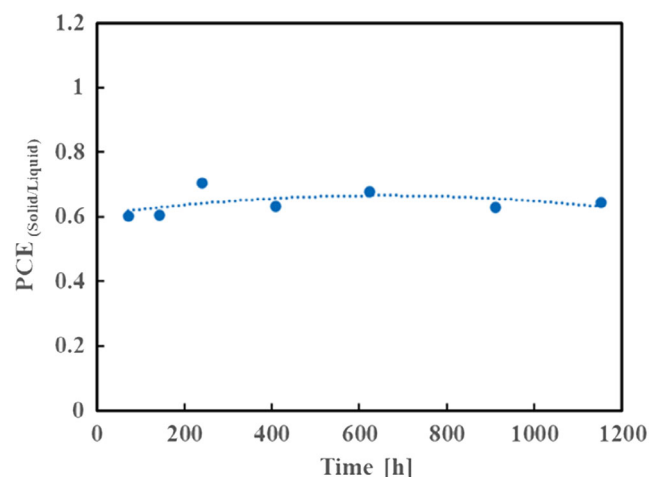


Figure 4. Time-dependent stability of ss-DSSC stored at room temperature. The concentration of the ionic liquid DMPIL used was 0.6 M.

ss-DSSCs at room temperature are shown in **Figure 4**. A perusal of this figure clearly corroborates that there was no significant change in the PCE of ss-DSSC after the electrolyte solidification corresponding to 72 h of natural solvent evaporation at room temperature. It is also evident from this figure that ss-DSSCs fabricated by the current method maintain about 60% of the PCE compared to liquid-state DSSCs for more than 1000 h. This suggests that ss-DSSCs being reported do not require special sealing contrary to perovskite solar cells and organic thin-film solar cells.

3.2. Optimization of Electrolyte Solidification for ss-DSSCs

In the present work, efforts were directed to fabricate ss-DSSCs via conventional liquid-state DSSC fabrication followed by its solidification by evaporation of the solvent of the electrolyte. Initially efforts were directed to fast solvent evaporation by opening the electrolyte injecting hole made on the counter electrode upon a hot plate at 90 °C and by applying a vacuum at room temperature. Both of the efforts were found to be futile and DSSC performances in both of the cases deteriorated sharply making devices nonfunctional. This led to a change in our direction of solidification from fast to slow and the effect of temperature on the solidification by solvent evaporation was investigated systematically by measuring the performances of liquid DSSCs and corresponding ss-DSSCs as a function time. Photovoltaic performances of the ss-DSSCs thus fabricated are shown in **Figure 5** followed by the summarization of photovoltaic parameters in **Table 1**. It can be seen from Figure 5 and Table 1 that observed V_{oc} in the case ss-DSSCs was slightly lower as compared to its liquid-state DSSC counterparts. The difference of V_{oc} between liquid-state and ss-DSSCs is considered partly to be due to the evaporation of tBP contained in the electrolyte controls the PCE of DSSCs by controlling the V_{oc} due to change in the quasi-Fermi energy level of TiO_2 .^[27]

At the same time, it can also be seen that FF in both the liquid-state and ss-DSSCs are only smaller as compared to the high efficiency reported in the literature but also it decreases with the increasing temperature for solidification. Especially this decrease was very high for solidification carried out at 80 °C. One of the

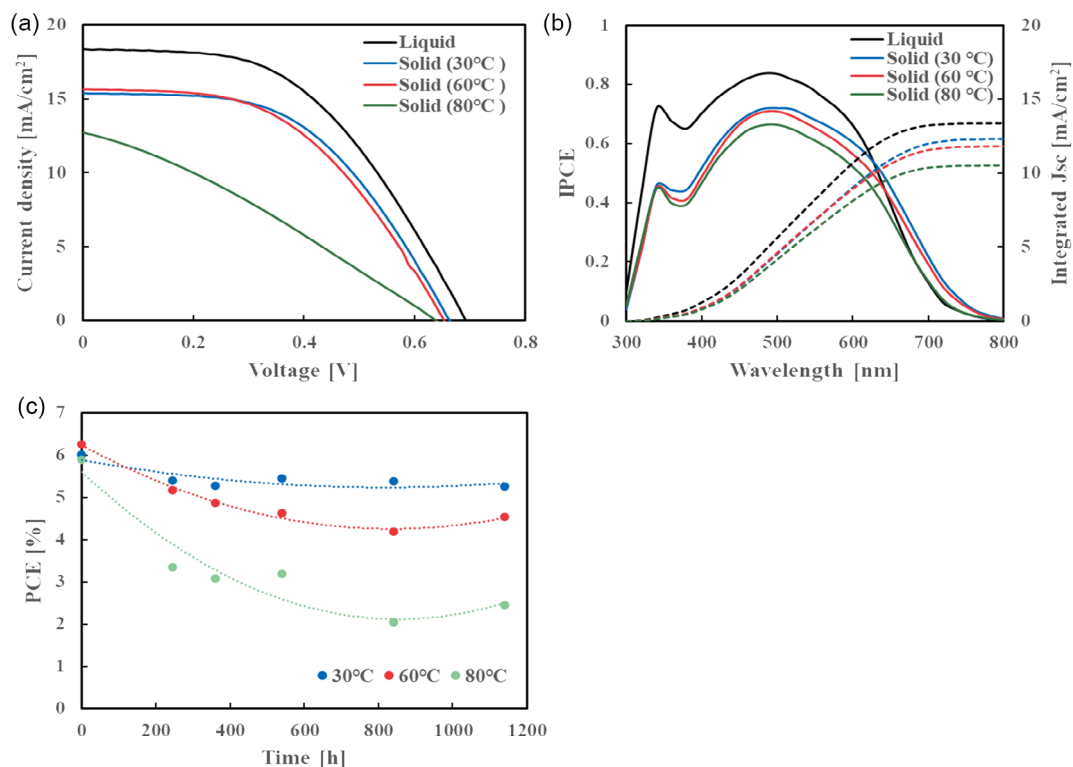


Figure 5. a) Photovoltaic performance; b) IPCE spectrum (solid line) and integrated photocurrent (dot line) of ss-DSSCs subjected for solidification at different temperatures and corresponding liquid-state DSSCs and time-dependent changes in the c) PCE for the ss-DSSC.

Table 1. Photovoltaic parameters for ss-DSSCs and corresponding reference liquid-state DSSCs subjected to solidification at different temperatures.

Temperature	State of DSSC	J_{sc} [mA cm^{-2}]	V_{oc} [V]	FF	PCE [%]	Integrated J_{sc} [mA cm^{-2}]
–	Liquid	18.4	0.700	0.487	6.27	13.3
30 °C	Solid	15.4	0.670	0.510	5.25	12.3
60 °C	Solid	14.6	0.650	0.477	4.53	11.8
80 °C	Solid	12.7	0.640	0.300	2.45	10.5

possible reasons for relatively poor overall FF is device structure, which is no-typical using a hot-melt spacer. In this work, the photoanode and counter electrode were directly affixed by UV resin without the use of hot melt spacers. The FF and V_{oc} were lower than those with spacers in the liquid-state DSSC, while J_{sc} increased. This decrease in the V_{oc} , as well as FF, might be attributed to improper contact with TiO_2 /electrolyte and counter electrode in the case of liquid electrolyte and inefficient ion-path/counter for ss-DSSCs. This was further validated by the fact that fast solidification carried out at 80 °C makes this contact more imperfect leading to the sharp decrease in the observed FF from 0.51 to 0.30.

The J_{sc} of 30 and 60 °C showed 15.4 and 14.6 mA cm^{-2} , respectively. On the other hand, 80 °C solidification showed 12.7 mA cm^{-2} , which was less than other conditions. These results can be confirmed by the IPCE spectra. There were no significant differences in the trend of the shape in the energy harvesting of the MK-2 from 400–700 nm in the IPCE spectra of the three conditions of SS-DSSCs. Therefore, it was suggested that these differences were not caused by the dye molecules being damaged by heating. It was caused by defects in the solid electrolyte formed by the rapid heating. The integrated J_{sc} from the IPCE curves was estimated to be 13.3 mA cm^{-2} (liquid-state), 12.3 mA cm^{-2} (30 °C), 11.8 mA cm^{-2} (60 °C) and 10.5 mA cm^{-2} (80 °C), respectively, which were slightly lower than the corresponding J_{sc} from the J - V characteristics, as shown in

Figure 5a and the data summary in Table 1. In fact, such relatively low integrated J_{sc} from IPCE has been reported in many reports. Possible reasons for this discrepancy include low monochromatic light intensity during IPCE measurements, recombination processes such as trapped states, the recombination nature, and space-charge effects.^[28] Zimmerman et al. reported that a difference of about 20% between the J_{sc} of the J - V characteristics under 100 mW cm^{-2} simulated solar irradiation and the integrated J_{sc} estimated from the IPCE spectrum shows a reasonable relationship.^[29] It can be seen from Figure 6 that solvent evaporation for solidification plays a dominant role in controlling not only the initial gap between the PCE of the liquid-state and ss-DSSCs but also long-term device stability too. High-temperature solvent evaporation carried out at 80 °C very fast removal of the solvent making nonhomogeneous distribution of polyiodide ions in the TiO_2 nanopores hampering the facile hole transport leading to fast deterioration of device performances as a function of time reaching about 30% of PCE for ss-DSSCs as compared to its initial value measured after 72 h. On the other hand, slow solvent evaporation carried out at room temperature (30 °C) not only retains about 80% of PCE for ss-DSSCs as compared to its liquid-state DSSC counterpart but also maintains the stability of ss-DSSCs for more than 1000 h remaining 90% of its initial PCE observed after 72 h of the storage of the ss-DSSC at the room temperature. This is attributed to the fact that solvent evaporation leads to uniform and continuous formation of polyiodide ions in the nanopores of the TiO_2 making facile dye-regeneration and swift hole transfer in the solid-state.

3.3. Implication of Ionic Liquid Concentration and Optimization of Electrolyte Solidification for ss-DSSCs

Electrolytes play a dominant role in the DSSCs working cycle not only by imparting the necessary ionic conductivity to the bulk of electrolyte solution but also by offering a reduction reaction at the counter electrode facilitating the dye regeneration by the charge-transfer reaction with the dye molecules.^[30] Apart from the use of iodine along with organic and inorganic iodides

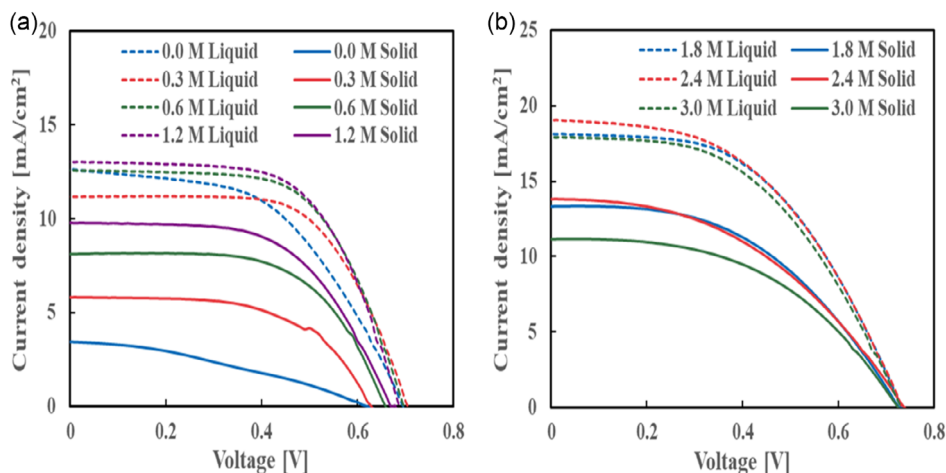


Figure 6. Photovoltaic performance of ss-DSSCs fabricated using DMP11 concentration varying from a) 0 to 1.2 M and b) 1.8 M to 3.0 M. The dotted lines represent the J - V curves for corresponding liquid-state DSSCs as reference.

to generate I^-/I_3^- redox couple in the most commonly used iodine-based redox electrolyte, several molten salts especially imidazolium cation-based ionic liquids have been used for improving the DSSC performances.^[31,32] In the case of utilizing imidazole-based ionic liquid, an increase in the concentration of imidazolium cations has been reported to decrease the recombination at the working electrode due to the multilayer adsorption finally leading to enhanced device performance.^[33] In an interesting report, Kubo et al. have also systematically investigated the effect of the alkyl chain and demonstrated that an increase in the alkyl chain length leads to an increase in the electron recombination lifetime owing to their enhanced hydrophobicity hampering the direct contact between the I_3^- ions and TiO_2 .^[34]

Among ionic liquids, those which are solid at room temperature are expected to be especially important in the formation of solid electrolyte. Taking this point into consideration, ionic liquid DMPII, which is solid at room temperature with a melting point of 94 °C was used for the fabrication and characterization of ss-DSSCs in this present work. The concentration of the ionic liquid in the electrolyte not only controls the charge carrier recombination as discussed above but also its optimum concentration is expected to form the creation of a facile ionic path in the nanopores of TiO_2 after solidification. This suggested a systematic investigation of the influence of ionic liquid concentration on the device performance and the durability of the ss-DSSCs fabricated using them. The $J-V$ curves for the liquid state and ss-DSSCs with varying concentrations of ionic liquid DMPII are shown in Figure 6 along with the summarization of photovoltaic parameters in Table 2.

A perusal of Figure 6 and Table 2 corroborates that using DMPII concentration of from 0 to 1.2 M, there was no significant difference in the device performance for liquid-state DSSCs with PCE varying from 4.5% to 5.5%. There was a monotonous increase in the PCE of ss-DSSCs as a function of the increasing

DMPII concentration. On the other hand, in the case of 0 M, DSSCs fabricated without using DMPII, PCE was drastically decreased (0.7) in the case of ss-DSSC as compared to its corresponding reference liquid state DSSC (4.5%). This hampering in the PCE of the ss-DSSC in the absence of DMPII was mainly due to highly suppressed J_{sc} as well as FF. When the concentration of DMPII was further increased from 1.8 to 3.0 M, there was a slight increase in the PCE for both the liquid-state and ss-DSSCs reaching a maximum PCE of 6.72% and 4.49% for the liquid-state and ss-DSSCs, respectively, with the 2.4 M of DMPII concentration. At the same time, it can be clearly seen from Table 2 that retention in the PCE for ss-DSSCs with respect to their corresponding liquid-state DSSCs counterparts increases with the increasing concentration of the ionic liquid DMPII and become saturated to the value of 69% after 1.2 M of DMPII.

Considering the saturation in the PCE for both solid-state and ss-DSSCs along with retention in PCE in solid-state after 1.8 M of DMPII concentration, efforts were directed to investigate the stability of ss-DSSCs fabricated in this 1.8 to 3.0 M and stored at room temperature for this higher DMPII concentration regime. Results of the PCE for the storage stability of the ss-DSSCs fabricated are shown in Figure 7. It can be clearly seen from this figure in all of the cases although ss-DSSCs exhibited their functionality and worked even after 1000 h of storage, the best device performance was demonstrated by the ss-DSSCs utilizing 2.4 M of DMPII with the maximum 60% retention in PCE after 1200 h.

4. Conclusion

Solid-state DSSCs utilizing the very simple method of slow solvent evaporation were fabricated followed by optimization of solidification conditions and ionic liquid concentration on the device performance and their storage stability. It has been shown that there was an increase in the J_{sc} as well as PCE for ss-DSSCs as a function of the increasing concentration of the ionic liquid DMPII used for electrolyte preparation. There was retention in the PCE for ss-DSSCs with respect to their corresponding

Table 2. Photovoltaic parameters for ss-DSSCs and corresponding reference liquid-state DSSCs utilizing different concentrations of ionic liquid DMPII.

Concentration [M]	State of DSSC	J_{sc} [$mA\ cm^{-2}$]	V_{oc} [V]	FF	PCE [%]
0.0	Liquid	12.6	0.700	0.508	4.49
0.0	Solid	3.45	0.630	0.333	0.72
0.3	Liquid	11.2	0.710	0.627	4.97
0.3	Solid	5.83	0.630	0.570	2.09
0.6	Liquid	12.6	0.700	0.614	5.41
0.6	Solid	8.12	0.660	0.609	3.26
1.2	Liquid	13.0	0.690	0.611	5.49
1.2	Solid	9.81	0.680	0.568	3.78
1.8	Liquid	18.1	0.740	0.501	6.72
1.8	Solid	13.3	0.730	0.475	4.62
2.4	Liquid	19.0	0.740	0.477	6.72
2.4	Solid	13.8	0.740	0.440	4.49
3.0	Liquid	17.9	0.740	0.485	6.42
3.0	Solid	11.2	0.730	0.483	3.94

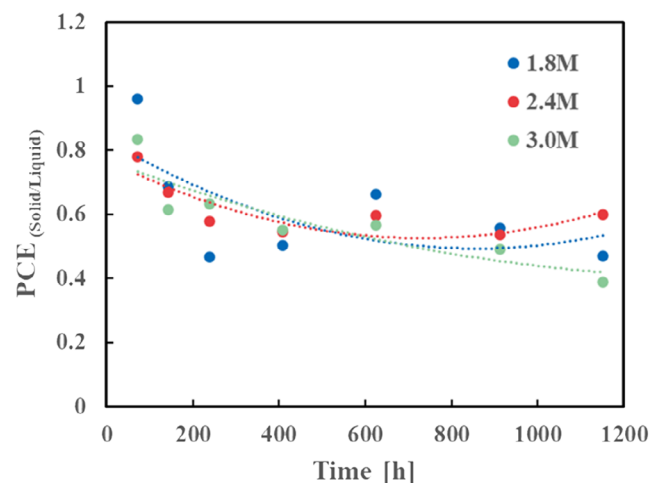


Figure 7. Storage stability of ss-DSSCs fabricated using the varying concentration of the DMPII from 1.8 to 3.0 M. PCE for ss-DSSCs was considered to be after 72 h of solvent evaporation at room temperature.

liquid-state DSSCs counterparts that increases with the increasing concentration of the DMPII and becomes saturated to the value of 69% after 1.2 M. In the case of ss-DSSCs with the ionic liquid concentration of 1.2 M, there was a good balance between PCE as well as durability leading to not only retention of about 70% of PCE as compared to its liquid-state DSSCs counterparts but also maintaining the stability of the solar cell for more than 1000 h stored at room temperature.

Acknowledgements

This work was supported by JST, the establishment of university fellowships toward the creation of science technology innovation, grant no. JPMJFS2133. One of the authors Y.K. would like to gratefully acknowledge the financial support under the Kyutech research fellowship.

Conflict of Interest

The authors declare no conflict of interest.

Data Availability Statement

The data that support the findings of this study are available from the corresponding author upon reasonable request.

Keywords

dye-sensitized solar cells, electrolyte solidification, iodide/triiodide redox, ionic paths, MK-2 dye

Received: February 21, 2023

Revised: August 4, 2023

Published online: October 25, 2023

- [1] N. S. Lewis, D. G. Nocera, *Proc. Natl. Acad. Sci. U.S.A.* **2006**, *103*, 15729.
- [2] M. Kokkonen, P. Talebi, J. Zhou, S. Asgari, S. A. Soomro, F. Elsehrawy, J. Halme, S. Ahmad, A. Hagfeldt, S. G. Hashmi, *J. Mater. Chem. A* **2021**, *9*, 10527.
- [3] C. Zhao, J. Wang, J. Jiao, L. Huang, J. Tang, *J. Mater. Chem. C* **2020**, *8*, 28.
- [4] Y. Chen, L. Zhang, Y. Zhang, H. Gao, H. Yan, *RSC Adv.* **2018**, *8*, 10489.
- [5] A. N. B. Zulkifili, T. Kento, M. Daiki, A. Fujiki, *J. Clean Energy Technol.* **2015**, *3*, 382.
- [6] M. Freitag, J. Teuscher, Y. Saygili, X. Zhang, F. Giordano, P. Liska, J. Hua, S. M. Zakeeruddin, J. E. Moser, M. Grätzel, A. Hagfeldt, *Nat. Photonics* **2017**, *11*, 372.
- [7] A. Hagfeldt, G. Boschloo, L. Sun, L. Kloo, H. Pettersson, *Chem. Rev.* **2010**, *110*, 6595.
- [8] M. Z. Molla, A. K. Baranwal, G. Kapil, S. Hayase, S. S. Pandey, *Sol. Energy* **2020**, *208*, 411.
- [9] M. Z. Molla, A. K. Baranwal, S. Hayase, S. S. Pandey, *ACS Appl. Electron. Mater.* **2020**, *2*, 2721.
- [10] A. K. Baranwal, N. Fujikawa, T. Nishimura, Y. Ogomi, S. S. Pandey, T. Ma, S. Hayase, *J. Phys. Conf. Ser.* **2016**, *704*, 012003.
- [11] G. S. Selopal, H. P. Wu, J. Lu, Y. C. Chang, M. Wang, A. Vomiero, I. Concina, E. W. G. Diau, *Sci. Rep.* **2016**, *6*, 18756.
- [12] M. Z. Molla, N. Mizukoshi, H. Furukawa, Y. Ogomi, S. S. Pandey, T. Ma, S. Hayase, *Prog. Photovoltaics Res. Appl.* **2015**, *23*, 1100.
- [13] U. Ahmed, M. Alizadeh, N. A. Rahim, S. Shahabuddin, M. S. Ahmed, A. K. Pandey, *Sol. Energy* **2018**, *174*, 1097.
- [14] A. Yella, H. W. Lee, H. N. Tsao, C. Yi, A. K. Chandiran, M. K. Nazeeruddin, E. W. G. Diau, C. Y. Yeh, S. M. Zakeeruddin, M. Grätzel, *Science* **2011**, *334*, 629.
- [15] K. Kakiage, Y. Aoyama, T. Yano, K. Oya, J. I. Fujisawa, M. Hanaya, *Chem. Commun.* **2015**, *51*, 15894.
- [16] J. M. Ji, H. Zhou, Y. K. Eom, C. H. Kim, H. K. Kim, *Adv. Energy Mater.* **2020**, *10*, 2000124.
- [17] S. Mathew, A. Yella, P. Gao, R. Humphry-Baker, B. F. E. Curchod, N. Ashari-Astani, I. Tavernelli, U. Rothlisberger, M. K. Nazeeruddin, M. Grätzel, *Nat. Chem.* **2014**, *6*, 242.
- [18] I. Benesperi, H. Michaels, M. Freitag, *J. Mater. Chem. C* **2018**, *6*, 11903.
- [19] H. Iftikhar, G. G. Sonai, S. G. Hashmi, A. F. Nogueira, P. D. Lund, *Materials* **2019**, *12*, 1998.
- [20] J. Zhang, N. Vlachopoulos, M. Jouini, M. B. Johansson, X. Zhang, M. K. Nazeeruddin, G. Boschloo, E. M. J. Johansson, A. Hagfeldt, *Nano Energy* **2016**, *19*, 455.
- [21] H. J. Snaith, L. Schmidt-Mende, *Adv. Mater.* **2007**, *19*, 3187.
- [22] A. Dualeh, F. De Angelis, S. Fantacci, T. Moehl, C. Yi, F. Kessler, E. Baranoff, M. K. Nazeeruddin, M. Grätzel, *J. Phys. Chem. C* **2012**, *116*, 1572.
- [23] I. Chung, B. Lee, J. He, R. P. H. Chang, M. G. Kanatzidis, *Nature* **2012**, *485*, 486.
- [24] Y. Cao, Y. Saygili, A. Ummadisingu, J. Teuscher, J. Luo, N. Pellet, F. Giordano, S. M. Zakeeruddin, J. E. Moser, M. Freitag, A. Hagfeldt, M. Grätzel, *Nat. Commun.* **2017**, *8*, 15390.
- [25] C. J. T. de Grotthuss, *Biochim. Biophys. Acta, Bioenerg.* **2006**, *1757*, 871.
- [26] E. Tanaka, N. Robertson, *J. Mater. Chem. A* **2020**, *8*, 19991.
- [27] J. Y. Kim, J. Y. Kim, D. K. Lee, B. Kim, H. Kim, M. J. Ko, *J. Phys. Chem. C* **2012**, *116*, 22759.
- [28] J. A. Christians, J. S. Manser, P. V. Kamat, *J. Phys. Chem. Lett.* **2015**, *6*, 852.
- [29] E. Zimmermann, P. Ehrenreich, T. Pfadler, J. A. Dorman, J. Weickert, L. Schmidt-Mende, *Nat. Photonics* **2014**, *8*, 669.
- [30] E. Stathatos, P. Lianos, S. M. Zakeeruddin, P. Liska, M. Grätzel, *Chem. Mater.* **2003**, *15*, 1825.
- [31] P. Wang, S. M. Zakeeruddin, I. Exnar, M. Grätzel, *Chem. Commun.* **2002**, *24*, 2972.
- [32] P. Wang, S. M. Zakeeruddin, P. Comte, I. Exnar, M. Grätzel, *J. Am. Chem. Soc.* **2003**, *125*, 1166.
- [33] S. Kambe, S. Nakade, T. Kitamura, Y. Wada, S. Yanagida, *J. Phys. Chem. B* **2002**, *106*, 2967.
- [34] W. Kubo, S. Kambe, S. Nakade, T. Kitamura, K. Hanabusa, Y. Wada, S. Yanagida, *J. Phys. Chem. B* **2003**, *107*, 4374.